

Extended Elastic Impedance concept as a simple tool to monitor producing reservoirs

Sergey Shevchenko

Curtin University, Perth, Western Australia
sergey.shevchenko@postgrad.curtin.edu.au
sergeys@sis-exploration.com

Wayne D. Pennington

Michigan Technological University, Houghton, Michigan
wayne@mtu.edu

SUMMARY

The Extended Elastic Impedance (EEI) concept has been used by the oil industry primarily for lithology and fluid prediction in exploration and development projects. We proposed a method of reservoir monitoring that identifies and maps changes in pressure and saturation in a producing reservoir by applying EEI to time-lapse seismic data. The method uses time-lapse seismic difference data rotated to specific EEI χ angles which have been optimised for the changes expected in a given reservoir.

In one approach to the problem, one angle is found to be appropriate to identify predicted changes in saturation, using fluid-substitution models, while the other angle is found from rock-physics assumptions or laboratory measurements of fluid-pressure changes. This technique was tested using time-lapse seismic data for the Enfield oil field, in the North West Shelf, Australia, with estimates of optimal EEI rotation angles χ based on log data and Biot-Gassmann modelling for the fluid changes, and on rock physics models fit to measurements made on core samples for the pressure changes. Seismic reflectivity and inversion domains were used for comparison and analysis of the final rotated volumes.

In addition to the approach described above, the optimal angles can be found from the scanning method that can be used as an express analysis in finding optimal χ angles for pressure and saturation changes in the producing reservoir.

Key words: Reservoir monitoring, Time-lapse seismic, Extended Elastic Impedance, Producing reservoir, Pressure change, Saturation change.

INTRODUCTION

One of the main objectives in the field development of hydrocarbon reservoirs is a change in pressure and saturation during production. Monitoring of producing reservoirs using time-lapse seismic data has been of interest for many geoscientists from late 90s.

Tura and Lumley (1999) developed method based on angle dependency of P-wave reflection amplitudes using pre-stack inversion for both P-wave and S-wave impedance changes over the reservoir. They applied P-wave AVO using pre-stack inversion that inverted for impedance changes of both P-waves and S-waves. Brevik (1999) presented a least-squares inversion method based on a rock physics model to invert P- and S-wave travel time differences for pressure and saturation changes. Cole et al., (2002) introduced a method to estimate pressure and saturation from 4D seismic pre-stack data attributes based on a nonlinear rock physics forward modelling inversion method using P and S time-lapse impedance changes as an inversion input. Lumley et al., (2003) developed a crossplot inversion method to estimate pressure and saturation changes using time-lapse seismic attributes. Saul and Lumley (2015) also studied changes in pressure at Enfield 4D seismic data. They proposed a method based on rock physics diagnostics to define the pressure sensitivity of rock properties including changes in the grain contact cement. The efforts to apply EEI to time-lapse seismic data were presented by Dai and Mei (2014), who briefly presented an application for the estimation of fluid saturation and pressure changes, and Chakraborty et al. (2020), who used modelled log data in a hypothetical case.

EEI methodology has been used in the exploration and development projects for the oil and gas industry for the last twenty years. It was introduced by Whitcombe (2002) and mainly has been used for lithology and fluid prediction using AVO analysis of seismic data. He extended the linearised EI AVO crossplot projections, initially introduced by Connolly (1999) and Hendrickson (1999), by relating the angle of incidence, θ , to an angle of axis-rotation, χ by $\sin^2 \theta = \tan \chi$. In this new domain of EEI the projections can be rotated from -90° to $+90^\circ$ through the rotation angle χ :

$$EEI(\chi) = V_{p0} \rho_0 [(V_p/V_{p0})^p (V_s/V_{s0})^q (\rho_p/\rho_0)^r], \quad (1)$$

where V_{p0} = average V_p , V_{s0} = average V_s , ρ_0 = average ρ , $\rho = \cos \chi + \sin \chi$, $q = -8k \sin \chi$, $r = \cos \chi - 4k \sin \chi$.

Whitcombe et al. (2002) demonstrated that important rock-physics parameters correspond to optimal χ angles: bulk modulus $\chi=+12.4^\circ$ and Lamé's parameter $\chi=+19.8^\circ$ but both can be within the range from $\chi=+10^\circ$ to $\chi=+30^\circ$. The shear modulus corresponded to $\chi=-51.3^\circ$ (Table 1) but could be within the range $\chi=-30^\circ$ to $\chi=-90^\circ$ depending on petrophysical properties of the formation. Those authors proposed using angles $\chi=+12.4^\circ$ and $\chi=-51.3^\circ$ to discriminate geological parameters such as fluid and lithology respectively. This concept is commonly used in exploration and field development studies.

The challenge in time-lapse studies is not to find lithology (which presumably does not change), but changes in pressure and in saturation; the angles appropriate for these may or may not be similar to those angles that are useful for exploration and development.

METHODOLOGY

We proposed (Shevchenko and Pennington, 2022) a method to use time-lapse seismic data in order to differentiate fluid changes from pressure changes, based on EEI for pre-stack seismic data, using angle rotations designed to optimize observation of changes these two parameters. We used the angle rotations from $\Delta R0$ (Intercept) and ΔG (Gradient) domains as the difference of Monitor survey minus Base survey observing the amplitudes from the seal-reservoir interface interpreted for both volumes. The optimal EEI rotation angle $\chi = +42^\circ$ for the fluid changes was estimated using log data and Biot-Gassmann modelling. The calculation of the optimal angle $\chi = -79^\circ$ for pressure changes was based on rock-physics models fit to measurements made on core samples from the well. Our observations we also compare with the results from the other methods and authors summarised in the Table 1.

Deterministic approach to finding appropriate angles. We recognised that the shear modulus is unaffected by fluid changes in the formation, as assumed in Biot-Gassmann modelling, but the shear modulus is affected by changes in effective confining pressure; as a result, a time-lapse change observed in EEI at an angle corresponding to shear modulus should indicate changes in effective confining pressure, and not changes in fluid content. An angle that is 90° from this should be sensitive (although perhaps not optimally so) to changes in fluid content and not to changes in effective confining pressure.

Scanning approach to finding appropriate angles. In addition to the methodology of Shevchenko and Pennington (2022), described briefly above, there is a seismic-data driven approach based on scanning through the EEI volumes calculated from -90° to $+90^\circ$ χ angles to find the optimal angles for changes in pressure and fluids. The method is a technically simple approach that utilizes the time-lapse seismic amplitudes differences that qualitatively satisfy conditions for the producing reservoirs described. Our initial idea to use this method was to test our deterministic approach results. Scanning the values of specific property changes that are of interest (pressure and saturation changes) from -90° to $+90^\circ$ χ angles, we expected to see the maximum values (extremums) on the graphs that would relate to optimum angles.

Details of the scanning approach We choose three areas as the polygons within the producing field with the specific conditions that can be tested by our method quantitatively. Polygon A is in the vicinity of the producer wells, equally away from the southern and northern injectors (Figure 1a); here we anticipated only small changes in either the pressure or saturation. Polygon B is within the oil leg just above the OWC where we expect an increase in both water saturation and pressure due to the nearby injector ENB01. Polygon C is within the water leg and close to injector ENB01 where we anticipate a large increase in pressure but no change in saturation. We calculated the rotated Intercept/Gradient volumes for every 10° on average, "scanning" from -90° to $+90^\circ$ for both Base (Base1P) and Monitor (M1P) surveys. Then we calculate the difference (M1P-Base1P) seismic reflectivity amplitudes from the Macedon shale and Macedon sand interface as the average for the polygons A, B and C (Figure 2) (Shevchenko, 2023).

CASE STUDY

The Enfield oil field, which is no longer under production, is located in the offshore Carnarvon Basin in Western Australia. The field is a north-easterly dipping structure sealed laterally by two major normal faults (Figure 1). The reservoir rocks are Late Jurassic "soft" Macedon Sandstone of average 24% porosity sealed by "hard" Macedon Mudstone. The reservoir consists of an Upper Reservoir of amalgamated turbidites with 10-25m thickness and a Lower Reservoir of locally developed channelised turbidites with thicknesses of over 50m. The two are separated by 1-2m thick shales interpreted as a major flooding surface. Numerous faults combined with the thin reservoir and a complex depositional architecture create limited fluid flow pathways, baffles and barriers that are difficult to predict (Hampson, 2012; Smith et al. 2008).

The base seismic survey was conducted in 2004 (BaseP), prior to development of the field. At the time of the monitor acquisition used here, in 2007 (M1P) (seven months after the field commenced oil production), the field had 3 horizontal and 2 deviated oil producers, 2 gas injectors in the gas cap, 3 deviated water injectors at the OWC and 3 deviated water injectors at the gas-oil-contact (GOC) (Figure 1a).

The seismic data that was used consisted of partial stacks at near (8°-18°), mid (19°-30°) and far (30°-41°) angle ranges and is of only fair quality for AVO application (Chan et al., 2009). The partial stacks were used to calculate seismic reflectivity Intercept and Gradient attribute volumes to compute AVA rotated volumes.

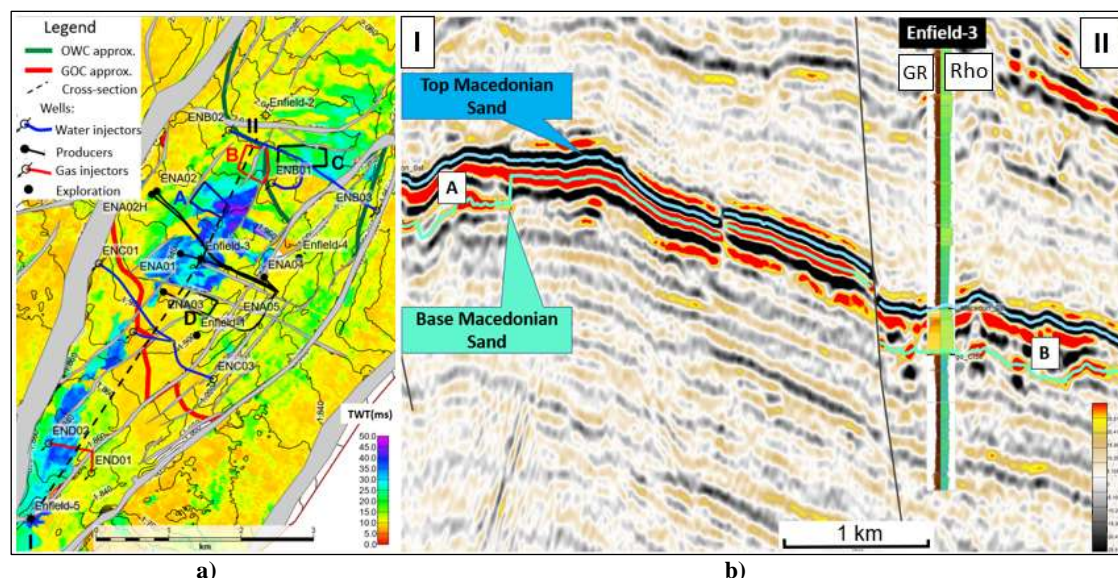


Figure 1. a) Enfield two-way time structural map shown as labelled contours to Top Macedon sandstone (ms) with colour representing isopach thickness of the Macedon sand reservoir. The labelled polygons (A, B, C, D) are areas in which quantitative studies were conducted, and injection and production wells at the time of Monitor survey are shown. Thin-bed artifacts in the seismic data are likely to be present where isopach thicknesses are less than 10 ms. b) Interpretation of the Top and Base Macedonian sand reservoir on the seismic cross-section I-II on a) through the well Enfield-3. Thick channelised turbiditic sequence shown as A and B.

Method of calculating EEI χ angle	Optimal χ angle (degree) for parameters				
	K	Mu	Lambda	Fluid	Pressure
Commercial software for Enfield wells	+13	-60	+21		
Whitcombe et al., (2002), for Gardner's parameters	+12	-51.3	+19.8		
Smith et al., (2008), using Enfield wells data				+60	-50
Gassmann Fluid Substitution using logs				+42	
Rock-physics model from core samples laboratory data					-70
Scanning, IntGrad volume χ rotation from -90° to +90°				+41	-50

Table 1. EEI optimal γ angles for rock-physics parameters from different sources and methods.

ANALYSIS AND RESULTS

First, we examine average values for fluid saturation changes in the polygons A, B and C (Figure 2). We expected maximum difference amplitudes (positive values) for polygon B (with maximum saturation change from oil to water) to be close to the angle $\chi=+42^\circ$ that we found for saturation change only from the Gassmann fluid substitution method. However, there is no extremum on the graph for polygon B related to positive values as we expected, instead, the graph increases towards $+90^\circ$ together with graphs for C and A polygons. But we see that the angle $\chi=+41^\circ$ on the graph is the only angle where the saturation change for polygon C (here, we do not expect saturation change) is 0. The change in saturation is also close to 0 for polygon A (here, we also do not expect saturation change), and there is a large positive difference for polygon B at this angle. The correct answer to optimal angle for saturation changes is in a combination of three polygon values that fit the conditions change for three polygons, which in our case is $+41^\circ$.

For the pressure case, the statistical graph shows the maximum amplitude (negative values) for polygon B is at $\chi=-79^\circ$, for polygon C is at $\chi=-55^\circ$ and for A is at $\chi=-50^\circ$. According to our prediction, maximum pressure without the effect of saturation should be observed at polygon C with a maximum value that is at the angle $\chi=-55^\circ$ on the graph. Although this angle does not coincide with our calculated angle for pressure change from the rock-physics model ($\chi=-79^\circ$), -55° is nearly orthogonal to $+42^\circ$ and close to the shear modulus angle -60° . We know that the larger angles are less reliable based on NRMS analysis (Shevchenko and Pennington, 2022), so this amount of disagreement is not surprising.

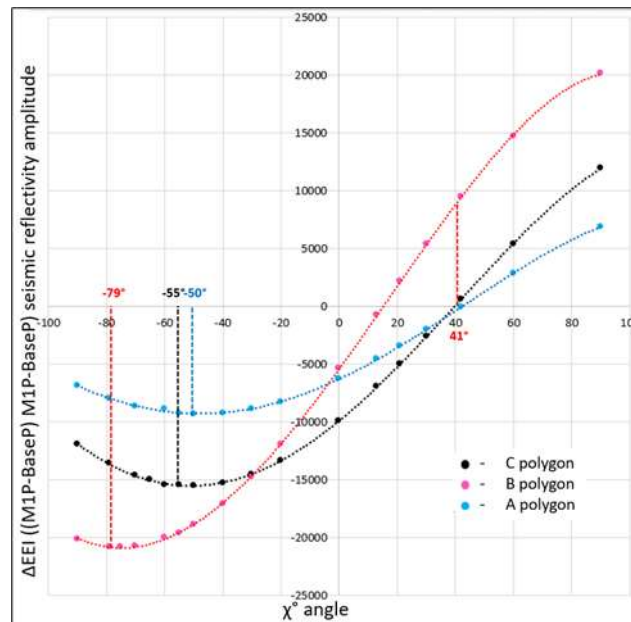


Figure 2. Intercept/Gradient AVA seismic amplitude (as average values) difference (M1P-Base1P) for Top Macedonian vs χ angles from -90° to $+90^\circ$ for A, B and C polygons.

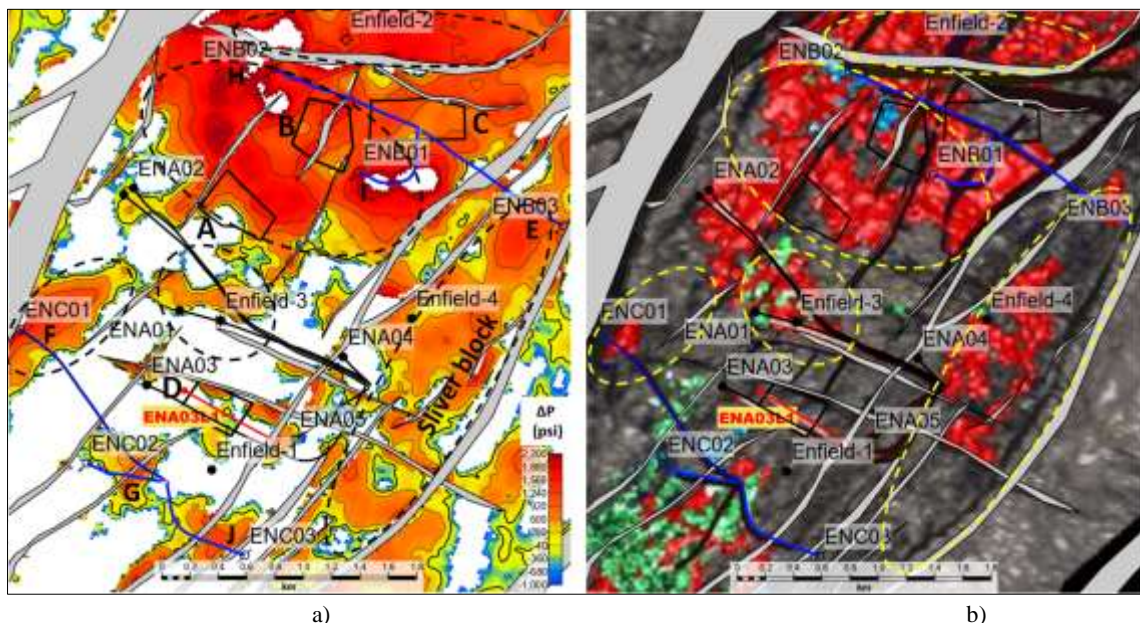


Figure 3. a) Reservoir fluid-pressure change ΔP (psi). Contour interval $\Delta P=500$ psi. Thick contour is 0. White color represents null values. (Polygon D was added for quality control for comparison with pressure obtained during drilling of well ENA03L1 (from Shevchenko and Pennington, 2022)). b) Reservoir pressure change (red) and Water saturation change (blue) map using volume interpretation based on Acoustic Impedance and Poisson Ratio cross-plotting performed by operator (Woodside Energy) modified from Smith (2008). The corresponding anomalies from two interpretations are highlighted by black and yellow ellipses respectfully. (a) and (b) maps are geographically rectified.

Figure 3a presents the final reservoir pressure (pore) change map calculated for $\chi=-79^\circ$ angle from the rock physics model (Shevchenko and Pennington, 2022). The map shows that all water injectors including ENC01, ENC02, ENB02, ENB01, ENC03 and ENB03 have anomalous pressure around the wells labelled F, G, H, I, J, and E, respectively. It is worth drawing attention to the pressure anomaly over the Sliver block on Figure 3a. The operator recognized (Smith, 2008) the pressure increase at this block and drilled a producer well updip of ENB03 in 2008 to recover unswept oil from this block (Hamson, 2012). The image in Figure 3b is shown for comparison as the reservoir pressure change (red) using volume interpretation based on Acoustic Impedance and Poisson Ratio cross-plotting performed by the operator Woodside Energy using the same seismic data (Smith, 2008). The corresponding anomalies from two interpretations are highlighted by black and yellow ellipses respectfully.

The movable-oil-saturation change ΔSwM map generated from our reflectivity volumes for $\chi=+42^\circ$ angle (Figure 4) (Shevchenko and Pennington, 2022) also correlates well with the expected increase in saturation around water injection wells at K (well ENC01), L (well ENC02), M (well ENB02) and J (well ENB03) above OWC. Anomaly L is worth emphasising as it likely caused water encroachment resulting in the shutting down of producer ENA03 and injector ENC02, consistent with the operator's interpretation (Smith et al., 2008). Thin beds (see Figure 1a) in the vicinity of the ENB01 injector below OWC present artefacts that appear as an (unreasonable) increase in saturation within the water leg.

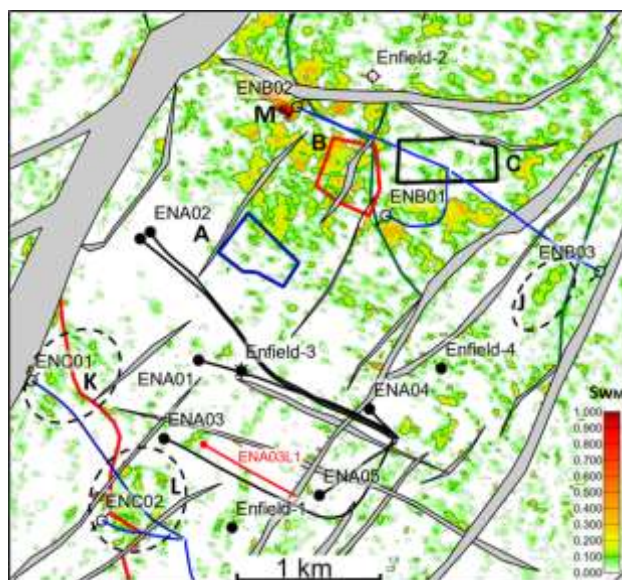


Figure 4. Movable-oil-saturation change ΔSwM . Solid highlighted contour $\Delta SwM=0.1$.

CONCLUSIONS

In a case study, the EEI method successfully predicted the areas where changes in pressure and/or saturation were expected, and did a good job of separating the two properties. Additionally, our anomalies of pressure and saturation change coincide with the results from operator and other researchers who used different methods to map pressure and saturation changes for the field. The scanning technique presented here could be useful for routine and fast analysis of time-lapse seismic data to identify appropriate EEI angles to use for separation of pressure and saturation effects.

ACKNOWLEDGMENTS

DownUnder GeoSolutions and GeoSoftware/HampsonRussell are gratefully acknowledged for providing interpretation software for this project. WDP acknowledges the support of Fulbright Australia and Curtin University.

REFERENCES

- Brevik, I., 1999, Rock model-based inversion of saturation and pressure changes from time-lapse seismic data, 69th Annual International Meeting: Society of Exploration Geophysics, 1044–1047.
- Chakraborty, S., R. Chatterjee, and A. Yadav, 2020, Time lapse rock physics template and seismic quantitative analysis amid the production phase: Journal of Applied Geophysics, 174, 103956, <https://doi.org/10.1016/j.jappgeo.2020.103956>.
- Chan, C., J. Sun, S. Birdus, K. M. Lee, O. Tang, and M. Wang, 2009, CGGVeritas, Veritas Geophysical (Asia Pacific) Pty Ltd, Enfield 4D survey, Northwest Cape, Western Australia, seismic data processing report.
- Cole, S., D. Lumley, M. Meadows, and A. Tura, 2002, Pressure and saturation inversion of 4D seismic data by rock physics forward modelling: 72nd Annual International Meeting: Society of Exploration Geophysics, Expanded Abstracts, pp. 2475–2478.
- Connolly, P., 1999, Elastic impedance: The Leading Edge, 18, no. 4, 438–452, <https://doi.org/10.1190/1.1438307>.

Hendrickson, J., 1999, Stacked: Geophysical Prospecting, 47, no. 5, 663–706, <https://doi.org/10.1046/j.1365-2478.1999.00150.x>.

Dai, X., and L. Mei, 2014, Time-lapse extended elastic impedance application in estimation of fluid saturation and pressure changes: International Geophysical Conference & Exposition, SEG and CPS, Global Meeting Abstracts, 974–977, <https://doi.org/10.1190/IGCBeijing2014-246>.

Hamson, G., 2012, Leveraging 4D seismic and production data to advance the geological model of the Enfield oil field, Western Australia: Search and Discovery Article 20172, adapted from oral presentation at Annual Convention and Exhibition, AAPG.

Lumley, D., M. Meadows, S. Cole, and D. Adams, 2003, Estimation of reservoir pressure and saturations by crossplot inversion of 4D seismic attributes: 73rd Annual International Meeting, SEG, Expanded Abstracts, 1513–1516.

Saul, M., and D. Lumley, 2015, The combined effects of pressure and cementation on 4D seismic data: Geophysics, 80, no. 2, WA135–WA148, <https://doi.org/10.1190/geo2014-0226.1>.

Shevchenko, S., (in press), 2023, Monitoring Pressure and Saturation Changes in a Clastic Reservoir from Time-lapse Seismic Data Using the Extended Elastic Impedance Method: Thesis for the degree of Doctor of Philosophy of Exploration Geophysics of Curtin University.

Shevchenko, S., and W. D. Pennington, 2022, Pressure and saturation changes estimated from extended elastic impedance properties using time-lapse seismic data: Enfield Field, NW Australia: The Leading Edge, 777–785, 41, no. 11, <https://doi.org/10.1190/tle41110777.1>.

Smith, M., 2008, Enfield 4D Monitor 1 2007 interpretation report, Woodside Company report.

Smith, M., A. Gerhardt, B. Mee, T. Ridsdill-Smith, A. Wulff, and L. Bourdon, 2008, The benefits of early 4D seismic monitoring to understand production related effects at Enfield, North West Shelf, Australia: 78th Annual International Meeting, SEG, Expanded Abstracts, 3159–3163, <https://doi.org/10.1190/1.3064002>.

Tura, A., and D. E. Lumley, 1999, Estimating pressure and saturation changes from time-lapse AVO data: 69th Annual International Meeting, SEG, Expanded Abstracts, 1655–1658, <https://doi.org/10.1190/1.1820849>.

Whitcombe, D. N., 2002, Elastic impedance normalization: Geophysics, 67, no. 1, 60–62, <https://doi.org/10.1190/1.1451331>.

Whitcombe, D. N., P. A. Connolly, R. L. Reagan, and T. C. Redshaw, 2002, Extended elastic impedance for fluid and lithology prediction: 70th Annual International Meeting, SEG, Expanded Abstracts, 138–141, <https://doi.org/10.1190/1.1815660>.